

# TRANSMUTATION FUEL CYCLE ANALYSES OF THE SABR FISSION-FUSION HYBRID BURNER REACTOR FOR TRANSURANIC AND MINOR ACTINIDE FUELS

C. M. SOMMER, W. M. STACEY,\* B. PETROVIC, and C. L. STEWART

*Georgia Institute of Technology, Nuclear and Radiological Engineering  
Atlanta, Georgia 30332*

Received May 6, 2011

Accepted for Publication July 9, 2012

*Fuel cycle analyses of the transmutation of (a) all of the transuranics (TRUs) in light water reactor (LWR) spent nuclear fuel (SNF) and of (b) the minor actinides (MAs) remaining in SNF (after separation of much of the plutonium for starting up fast reactors) have been performed for the conceptual subcritical advanced burner reactor (SABR) fission-fusion hybrid sodium-cooled fast burner reactor. Both metallic and oxide burner reactor fuels were considered, and the effect of clad radiation*

*damage limit on fuel residence time was investigated. For a radiation damage limit of 200 displacements per atom, the support ratio (LWR power/SABR power) for transmuting all of the TRUs produced by LWRs is 3/1, and for transmuting just the MAs produced by LWRs the support ratio is 25/1. The reduction in high-level waste repository capacity required due to this transmutation is a factor of 10, based on a decay heat at a 100 000-yr limit on capacity.*

## I. INTRODUCTION

At the present rate of nuclear power generation in the United States, enough spent fuel will have accumulated to fill a Yucca Mountain-type high-level radioactive waste repository (HLWR) by the year 2020 (Ref. 1). The forecast for increased power generation by nuclear power in the next 30 yr and over the coming century magnifies the issue of spent nuclear fuel (SNF) disposal. Between 2007 and 2010 the U.S. Nuclear Regulatory Commission (NRC) accepted applications for 26 new light water reactors (LWRs), and the NRC expects applications for another 5 reactors in 2011 (Ref. 2). These 31 reactors would increase the current nuclear power output of the United States by ~30%, increasing the amount of discharge fuel needed to be stored in geological repositories by a similar amount.

Until very recently, the reference U.S. option for disposal of SNF was (a) initially on-site storage and

(b) shipping the fuel to a geological repository where it would be interred forever. With this predicted increase in nuclear power, a new geological repository of the same size as Yucca Mountain would be needed every 45 yr.

A second option for spent fuel disposal is to introduce a multistrata fuel cycle in which following (a) initial on-site storage, (b) the spent fuel from LWRs is recycled in advanced burner reactor systems to burn essentially all the long-lived actinides that determine the requirement to demonstrate performance for a 100 000-yr interment, and (c) then only the fission products and trace amounts of actinides are sent to long-term HLWRs. The multistrata fuel cycle would not replace geological repositories but would significantly reduce the number of HLWRs that are necessary.

Such multistrata fuel cycles have been widely studied for critical advanced burner reactors and for subcritical reactors supported by an external source of neutrons provided by an accelerator target embedded in the core<sup>3</sup> and examined to a lesser extent for subcritical reactors supported by fusion neutron sources.<sup>4-7</sup>

\*E-mail: Weston.stacey@nre.gatech.edu

Utilizing subcritical reactors with a variable-strength fusion neutron source removes the criticality constraint on fuel residence time and allows for the fuel to remain in the reactor until the radiation damage limit is reached, which should result in fewer reprocessing steps and ultimately fewer repositories than would be needed in a multistrata fuel cycle utilizing critical burner reactors. The subcritical operation also provides an extra margin of safety to prompt critical, which should allow the burner reactor to be fueled with 100% transuranics (TRUs), instead of  $\sim 20\%$  TRUs for critical reactors, which should result in fewer subcritical than critical burner reactors being necessary to support a given fleet of LWRs. On the other hand, the subcritical reactor with a fusion neutron source would be more complex and expensive than a comparable critical reactor.

A fission-fusion hybrid is a subcritical fission reactor supplemented by a fusion neutron source. The fusion neutron source is chosen for three reasons. First, fusion is one of only two options for a copious neutron source; second, the fusion neutron source strength is variable and can be increased or decreased to maintain a desired fission or thermal power level independent of the changes in reactivity throughout the cycle; and third, the fusion neutron source is a distributed neutron source capable of irradiating a larger volume of fuel than a point neutron source such as an accelerator target, the other option for such a large neutron source.<sup>8</sup>

This paper focuses on various transmutation fuel cycles in the subcritical advanced burner reactor<sup>9</sup> (SABR), a fission-fusion hybrid reactor with a fusion neutron source based on ITER physics and technology<sup>10</sup> combined with a fast burner reactor based on the leading sodium-cooled fast reactor technology. Fuel residence time is limited in these fuel cycles by the radiation damage to the structural materials. This study examines three different fuel types [(a) TRUs from LWRs in a metallic fuel, (b) minor acti-

nide (MA)-rich TRUs from which some of the Pu has been removed in a metallic fuel, and (c) MA-rich TRUs in an oxide fuel] for transmutation in the SABR.

## II. SABR DESIGN

### II.A. Overview

Figure 1 is a simplified three-dimensional model of the SABR. The toroidal fusion plasma is surrounded on its outboard side by an annular subcritical TRU fission core. The fission core consists of four concentric annular rings formed by vertical hexagonal fuel assemblies, surrounding the plasma of the fusion neutron source. The active core is 0.64 m thick by 2.0 m in active height (plus a 1-m fission gas plenum) and produces 3000 MW (thermal) of thermal power (from fission, from thermal energy deposited by the fusion neutrons, and from exoergic nuclear reactions).

The annular core geometry is required by the neutron source geometry, but it may have some advantages, such as negative sodium void and fuel expansion reactivity coefficients. Moreover, an annular core does not seem to have any disadvantages relative to a cylindrical core—for the same fuel and power density, annular and cylindrical cores with equal transmutation (fission) rates would have the same volumes.

Slightly different core designs have been developed for three different fuel types. Two designs of metal fuel cores based on Integral Fast Reactor (IFR) technology<sup>11</sup> were developed, one based on the TRU-Zr metal fuel under development at Argonne National Laboratory<sup>12</sup> and the other based on a TRU-MgO metallic fuel with the reduced plutonium composition specified in European fuel cycle scenario studies.<sup>7</sup> The third fuel design is a TRU-MgO oxide fuel based on the same European fuel

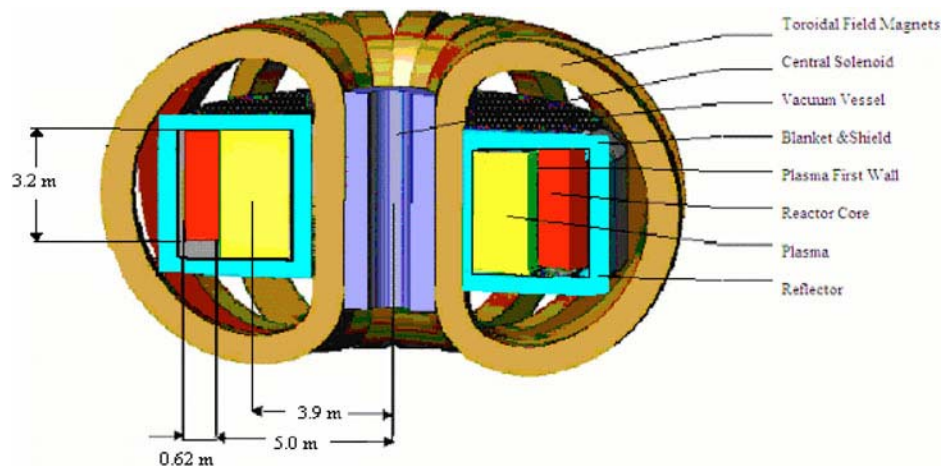


Fig. 1. Three-dimensional model of SABR.

composition. The Argonne TRU-Zr fuel composition is representative of the spent fuel discharged from LWRs, while the European TRU-MgO fuel composition is representative of a MA-rich fuel that would result after setting aside some of the plutonium from LWR spent fuel for future use in starting up fast reactors.

The plasma and core region are surrounded by a 15-cm lithium oxysilicate blanket for tritium production, followed by a steel reflector and a multilayered shield to capture neutrons and gamma rays and to protect the toroidal field magnets from radiation damage.

A detailed geometric cross section of SABR, illustrating the locations of these various regions, is shown in the  $r$ - $z$  neutronics computation model of SABR shown in Fig. 2. As a point of reference, SABR, with a plasma major radius  $<4$  m, is about half the size (by volume) of ITER (Ref. 9).

## II.B. Fuel Element and Fuel Assembly Design

Originally, SABR was designed<sup>9</sup> for the TRU-Zr metal fuel being developed by Argonne National Laboratory.<sup>12</sup> The fuel is composed of 40Zr-40Pu-10Np-10Am by weight percent. The isotopic composition of

the fuel is given in Table I. The metallic fuel form was chosen because it has a high thermal conductivity, has the possibility of achieving the inherent safety characteristics of the IFR (Ref. 11), and has a fuel cycle in which the plutonium is never separated from the higher actinides.

The fuel pins in SABR are based on a standard IFR-type metallic fuel pin design but coated with an electrical insulator to reduce the magnetohydrodynamic pressure drops associated with sodium coolant in a magnetic field.<sup>9</sup> (The design power density was significantly lower than the usual IFR designs, and the effect of the insulator on thermal performance was taken into account.) The SABR fuel pins based on the composition in Table I are shown in Figs. 3 and 4. The basic SABR fuel assembly with 271 of these fuel pins is shown in Fig. 5. The core consists of 918 such fuel assemblies arranged in four annular rings.

## II.C. SABR Fuel Assemblies for European MA-Rich Fuel

The Karlsruhe Institute of Technology is examining a fuel cycle scenario of interest to some European countries,<sup>7</sup> in which the plutonium is removed from spent fuel and set aside for future use, leaving the MA-rich fuel type shown in Table II. This fuel composition was

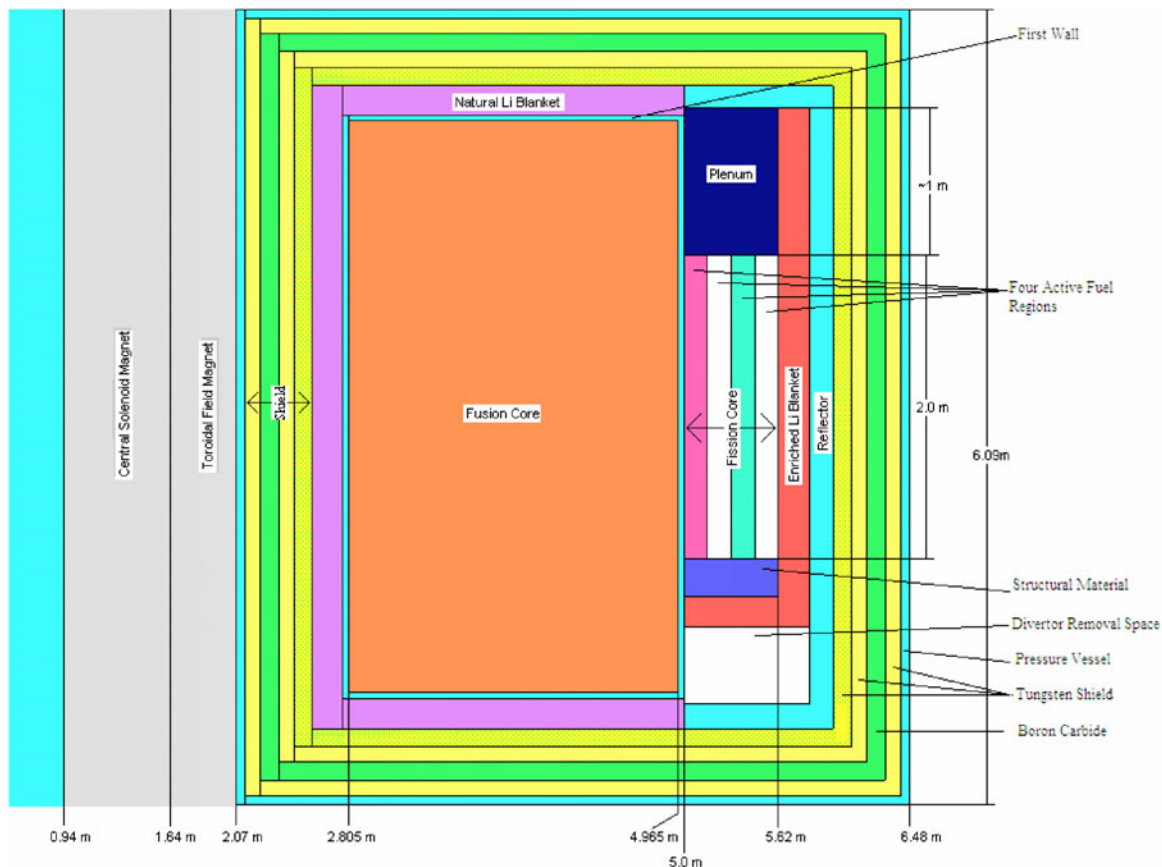


Fig. 2. SABR  $r$ - $z$  neutronics computational model.

TABLE I  
Argonne TRU Fuel Composition\*

Isotope	Mass Percent at BOL
Neptunium-237	17.0
Plutonium-238	1.4
Plutonium-239	38.8
Plutonium-240	17.3
Plutonium-241	6.5
Plutonium-242	2.6
Americium-241	13.6
Americium-243	2.8

\*Reference 12.

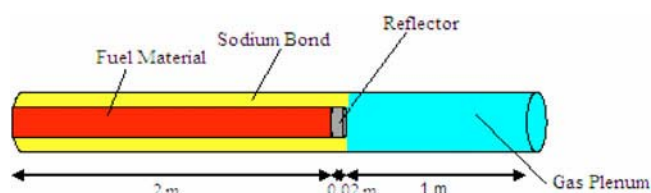


Fig. 3. Axial view of SABR fuel pin (not to scale).

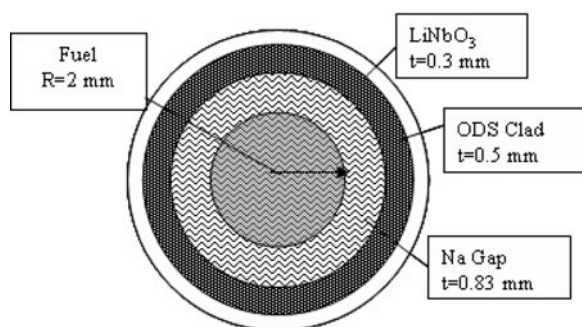


Fig. 4. Metal-TRU fuel pin; ODS = oxide dispersion strengthened.

selected<sup>8</sup> to have a minimal reactivity change with burnup to accommodate a subcritical burner reactor with an accelerator neutron source. The fuel consists of 45.7% plutonium and 54.3% MAs in a magnesium oxide matrix.

Two fuel types using the European fuel composition of Table II were examined. The first fuel type was a metal fuel. The same fuel pin and fuel assembly design described in Sec. II.B for the original SABR fuel were used, but with the fuel composition of Table II instead of that of Table I, and an oxide matrix rather than a zirconium matrix.

An oxide fuel with the MA-rich composition of Table II was also considered. Since the oxide fuel has a

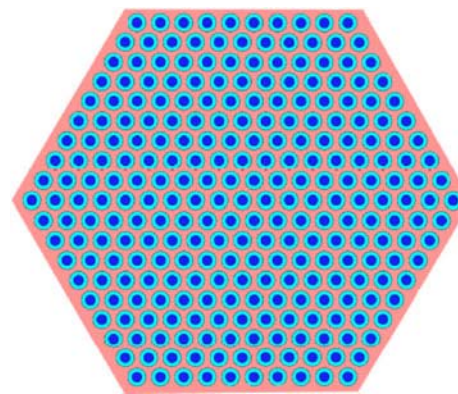


Fig. 5. Metallic fuel assembly (15.5 cm across flats).

TABLE II  
European MA-Rich Fuel Composition\*

Plutonium Vector		MA Vector	
Isotope	Mass Percent	Isotope	Mass Percent
Plutonium-238	3.737	Neptunium-237	3.884
Plutonium-239	46.446	Neptunium-239	0.0
Plutonium-240	34.121	Americium-241	75.51
Plutonium-241	3.845	Americium-242 <sub>m</sub>	0.254
Plutonium-242	11.85	Americium-242 <sub>f</sub>	0.000003
Plutonium-243	0.0	Americium-243	16.054
Plutonium-244	0.001	Curium-242	0.0
		Curium-243	0.066
		Curium-244	3.001
		Curium-245	1.139
		Curium-246	0.089
		Curium-247	0.002
		Curium-248	0.0001

\*Reference 8.

lower heavy metal density than metallic fuel, a larger fuel volume is needed to operate in the same range of  $k_{eff}$  as the metal fuel designs. The SABR fuel pins and fuel assemblies were slightly redesigned to accommodate the oxide fuel. The European fuel pin design from the EFIT study<sup>8</sup> was used for the oxide fuel, resulting in the oxide fuel pin having a larger pin diameter and a smaller coolant-to-fuel-volume ratio. This is possible because the oxide fuel has a much greater melting temperature than the metallic fuel, ~3000 K for oxide and 1350 K for metallic. The oxide fuel assembly has the same outer dimensions as the metallic fuel assembly but contains 217 fuel pins instead of 271. Each fuel pin with the oxide fuel has an outer pin diameter of 8.72 mm as compared to 7.36 mm for the metallic fuel. Figures 6 and 7 are representations of the oxide fuel pins and assembly, respectively.

A comparison of the major parameters for the oxide and the metal fuel pins and fuel assemblies is given in Table III.

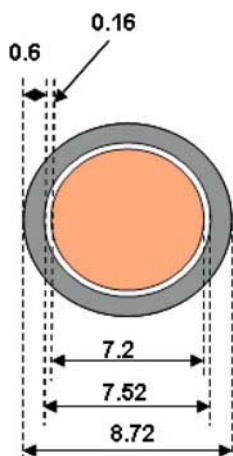
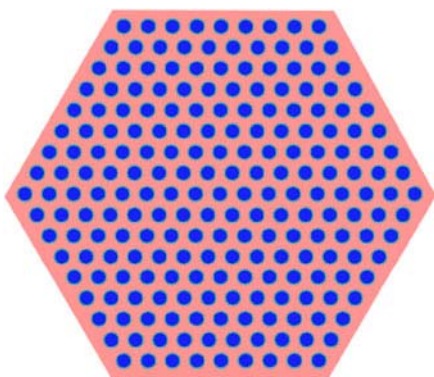
Fig. 6. Oxide fuel pin.<sup>8</sup>

Fig. 7. Oxide fuel assembly (15.5 cm across flats).

#### II.D. Fusion Neutron Source

Conservative ITER-like physics were adopted for the design of the SABR tokamak neutron source.<sup>13</sup> (By conservative, we mean that values of performance parameters that have already been achieved regularly in experiments were chosen for most physics design parameters, rather than the more favorable values anticipated in future experiments.) The neutron source was designed to produce a fusion power of  $P_{fus} = 100$  to 500 MW(thermal), which will be shown to be adequate to support the design objective of a total power in the fission core (from fission, fusion neutrons slowing down, and other exoergic reactions), of  $P_{fis} = 3000$  MW(thermal), under the range of subcritical operation envisioned.

The ITER technological systems were adapted for SABR. The ITER single null divertor (not shown in Fig. 1) and first wall were adapted for sodium coolant by scaling down to the SABR dimensions with the same coolant channels. The ITER lower hybrid heating and current drive system was used to provide 100 MW of heating and to drive

7.5 mega-amperes of plasma current. The superconducting magnet systems for SABR were scaled down<sup>13</sup> from the ITER design of magnets with a cable-in-conduit Nb<sub>3</sub>Sn conductor surrounded by an INCOLOY<sup>®</sup> alloy 908<sup>a</sup> jacket and cooled by a central channel carrying supercooled helium, with maximum fields of 11.8 and 13.5 T, respectively. The dimensions of the central solenoid coil were constrained by the requirement to provide inductive start-up and to not exceed a maximum stress of 430 MPa set by matching ITER standards and INCOLOY properties. The dimensions of the 16 toroidal field coils were set by conserving tensile stress calculated as for ITER, taking advantage of an INCOLOY alloy 908 jacket for support.

It is intended that the fusion neutron source strength would be adjusted slowly (every week or so, perhaps) to compensate for the reactivity change due to fuel burnup to maintain a relatively constant fission core power level and temperature distribution within the reactor. There are many ways this could be accomplished, although a specific operational scenario has not yet been developed. The plasma power balance can be altered by changing the amount of heating power into the plasma, by changing the fueling rate, and by other changes to the operating conditions that affect the rate at which energy and particles escape from the plasma. The present design has 20-MW auxiliary heating units, which are too large to affect small changes in the neutron source level, so some incremental megawatt-level heating sources would probably have to be included. The fueling is by opening a valve and pumping gas into the chamber, and the amount of gas can be readily controlled. There are many possibilities for changing the rate at which energy and particles escape from the plasma. Thus, altering the plasma neutron source level would seem to be practically feasible and should have no impact on availability.

#### III. SABR FUEL CYCLE

The SABR utilizes the out-to-in shuffling pattern depicted in Fig. 8.

At beginning of life (BOL), fresh fuel is placed in all four annular rings of the core. The fuel is irradiated for a burn cycle time and then shuffled inward by one ring, with the fuel in the innermost ring (ring 1 in Fig. 8) being removed from the core and sent to the reprocessing facility at the end of each burn cycle. Fresh fuel from the fabrication facility is loaded into the outermost ring, ring 4, and the fuel is irradiated for another burn cycle. This process is repeated, with the fuel composition fed into SABR soon reaching equilibrium.

In the reprocessing facility, the fission products are separated from the remaining TRUs (a conservative 99% separation efficiency is assumed). The fission products (and 1% of the TRUs) are sent to a HLWR. The remaining TRUs

<sup>a</sup>INCOLOY is a registered trademark of the Special Metals Corporation group of companies.

TABLE III

Key Design Parameters of Metal and Oxide Fuel Pins and Assemblies

Parameter	Metal	Oxide	Parameter	Metal	Oxide
Length of fuel rods (m)	3.2	3.2	Total pins in core	248 778	199 206
Length of active fuel (m)	2	2	Diameter, flat to flat (cm)	15.5	15.5
Length of plenum (m)	1	1	Diameter, point to point (cm)	17.9	17.9
Length of reflector (m)	0.2	0.2	Length of side (cm)	8.95	8.95
Radius of fuel material (mm)	2	3.6	Fuel rod pitch (mm)	9.41	13.63
Thickness of clad (mm)	0.5	0.3	Pitch-to-diameter ratio	1.3	1.56
Thickness of Na gap (mm)	0.83	0.16	Total assemblies	918	918
Thickness of LiNbO <sub>3</sub> (mm)	0.3	0.3	Pins per assembly	271	217
Radius of rod with clad (mm)	3.63	4.36	Coolant flow area per assembly (cm <sup>2</sup> )	96	108

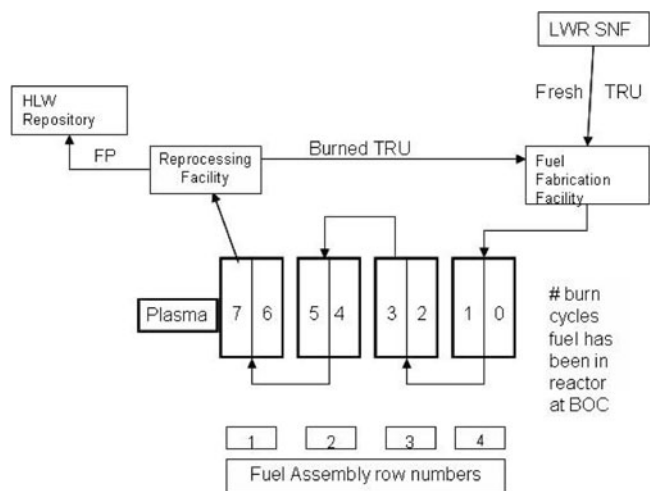


Fig. 8. The SABR fuel cycle.

(and 1% of the fission products) are sent back to the fuel reprocessing facility where they are combined with fresh TRUs from LWRs and sent to the fuel fabrication facility, where new fuel elements and assemblies are manufactured and then placed back into the reactor.

Fuel shuffling and successive reloading within the tokamak toroidal field coil configuration of Fig. 1 will be challenging and require some mechanical design ingenuity. Similar problems have been addressed by the ITER designers, who must provide for test assembly removal/insertion and for replacement of failed components in the same geometry. One can contemplate modular blocks of fuel assemblies, which are removed radially between toroidal field coils for refueling external to the coils, with blocks under the coils being rotated and then removed.

#### IV. FUEL CYCLE SIMULATIONS

A series of fuel cycle simulations was performed for the SABR transmutation system, to identify the charac-

teristics of two types of fuel cycle that could be accommodated in SABR: (a) a TRU-burning fuel cycle in which all of the TRUs in the spent fuel discharged from LWRs were burned, and (b) a MA-burning fuel cycle in which much of the plutonium from discharged LWR fuel was set aside for future use but all the MAs were burned. The length of the fuel cycle was determined by the radiation damage limit of the clad and structural material. Fuel cycles were examined with three different fuel types: metal-TRU, metal-MA, and oxide-MA, as described in Sec. II.

Each fuel cycle simulation was evaluated based on multiple performance indicators: burnup, total TRU destruction, total plutonium destruction, total MA destruction, required fusion power, power peaking, LWR support ratio, radiation damage, decay heat to the repository, etc.

The fuel cycle calculation was made with the ERANOS2.0 software package,<sup>14</sup> using JEFF2.0 cross sections in 33 energy groups from 20 MeV down to 0.1 eV. A lattice cell calculation in  $P_1$  transport theory and 1968 energy groups was performed on the fuel assembly, the energy groups were collapsed to 33 groups, and the assembly was then homogenized. The transport simulation in ERANOS was performed with BISTRO, a discrete ordinates transport solver.<sup>15</sup> The flux solution was calculated using an  $S_8$  quadrature set in the  $r$ - $z$  geometry of Fig. 2, with 91 radial and 94 axial mesh points. Fuel depletion was simulated with the EVOLUTION module.<sup>16</sup> EVOLUTION uses an average flux profile and depletes the fuel based on this profile for a given time period. To achieve an accurate isotopic burnup the fuel was depleted in 233-day time steps to account for the change in flux profile over time.

#### IV.A. Accumulated Radiation Damage Versus Burnup for Metal-TRU Fuel

The first fuel cycle issue examined was the effect of clad radiation damage limit on fractional fuel burnup in a fuel residence time. Simulations were run for the SABR

out-to-in shuffling pattern for irradiation times corresponding to 100, 200, and 300 displacements per atom (dpa), as well as for a hypothetical once-through fuel cycle with a radiation damage limit sufficient to achieve >90% burnup before the fuel is removed from the reactor. Radiation damage limits of 150 to 200 dpa are anticipated for clad and structural materials presently under development. The 300-dpa limit was investigated to determine if there is a strong incentive for developing new clad materials able to withstand a higher radiation damage dose. The once-through cycle was examined to determine what radiation damage limits would be needed to achieve high burnup of the TRU fuel without reprocessing and to examine the power distributions that would result in such a low reactivity core.

The simulations show that the relationship between radiation damage and burnup is linear in the regime from 100 to 300 dpa. This linear relationship results in linear increases in fusion power and TRUs burned per residence in this regime. The results are summarized in Table IV.

The TRU burnup rate depends on the fission rate, of course, and the fission rate decreased as the fusion rate increased to compensate for reactivity loss [recall that it is the total thermal power in the fission core that is held constant at 3000 MW(thermal)]. This accounts for the downward trend in TRUs burned per year from the 100-dpa cycle to the once-through cycle. As can be seen from Table IV, the ratio of fission power to fusion power in the recycling fuel cycles varies from >30 at BOL to ~7.5 at the end of the equilibrium fuel cycle (EOC).

Since a 1000-MW(electric) LWR produces ~250 kg of TRUs/yr, a support ratio of LWRs per SABR can be defined by dividing the SABR TRU destruction rate

by the LWR production rate. For this purpose, we assume that SABR operates at 75% availability, taking into account refueling downtime and unscheduled downtime.

The assembly-average power peaking (the assembly-average power in the first ring to the core-average power over all four rings) indicated in Table IV is generally <2.0. The power is relatively uniform, with peak-to-average factors of 2 or less, except for the once-through cycle where the very different composition of the fuel in adjacent rings produces large power peaking. The detailed power distribution is shown in Fig. 9 for EOC in the most limiting 300-dpa case.

The distribution of accumulated fast-neutron (>100 keV) fluence and the dpa at the end of the 300-dpa equilibrium cycle are plotted in Figs. 10 and 11, respectively.

The jumps in the distributions occur between rings of assemblies that have been in the reactor different numbers of burn cycles. This sort of ring-to-ring power peaking can be handled by flow zoning among the rings of assemblies,<sup>17</sup> and the within-assembly dpa gradient can be reduced by rotating the assemblies when they are shuffled between rings. No effort has been made yet to optimize the within-assembly power distribution.

The decay heat in the repository was calculated with ORIGEN-S (Ref. 18). Fast-group cross sections were imported into ORIGEN-S, and the fuel was then depleted under a constant flux until the burnup reached the same level of burnup seen in ERANOS. The calculation of decay heat to the repository was done assuming reprocessing separation efficiency of 1%, meaning 99% of the fission products and 1% of the TRUs go to the repository on each reprocessing step.

TABLE IV  
Summary of Radiation Damage Versus Burnup

Parameter	100 dpa	200 dpa	300 dpa	Once through
Cycle	100 dpa	200 dpa	300 dpa	Once through
Burn cycle length time (days)	350	700	1000	4550
Four-batch residence time (yr)	3.83	7.67	10.95	49.8
Fission power [MW(thermal)]	3000	3000	3000	3000
FIMA (%)	16.7	23.8	31.6	87.2
Region power peaking BOC/EOC	1.7/1.8	1.8/2.0	1.8/2.0	2.0/2.1
BOL $P_{fus}$ (MW)	73	73	73	73
BOC $P_{fus}$ (MW)	155	240	286	1012
EOC $P_{fus}$ (MW)	218	370	461	1602
BOL $K_{eff}$	0.972	0.972	0.972	0.972
BOC $K_{eff}$	0.940	0.894	0.887	0.784
EOC $K_{eff}$	0.916	0.868	0.834	0.581
TRUs burned/yr (kg)	1073	1064	909	545
Support ratio (75%)	2.9	3.2	3.6	2.2
Clad damage (dpa)	97	214	294	1537

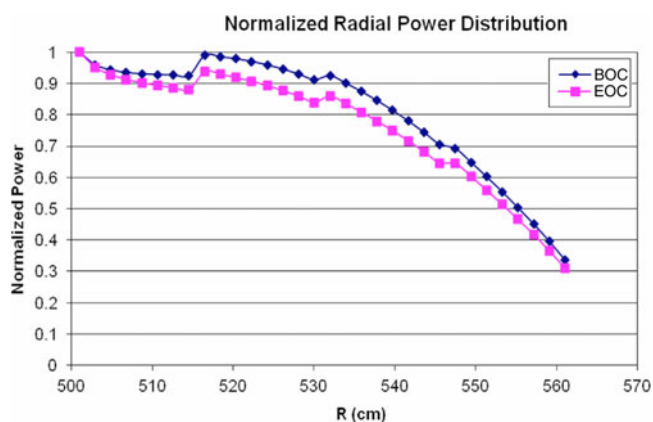


Fig. 9. Power distribution for the TRU burner fuel cycle at end of the 300-dpa equilibrium cycle.

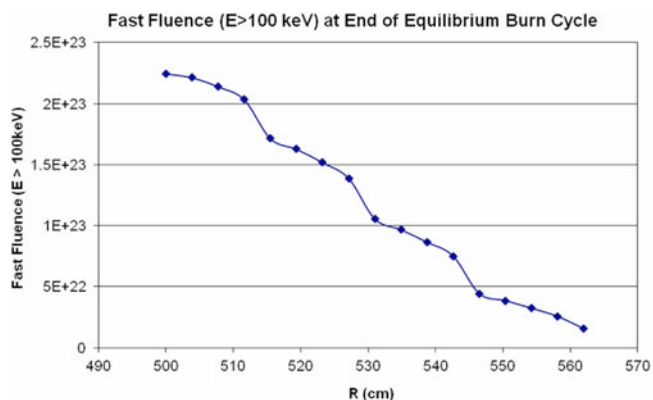


Fig. 10. Fast-neutron fluence at end of the 300-dpa equilibrium fuel cycle.

Figure 12 shows the decay heat to the repository for each of the four TRU burner fuel cycles, as well as for unprocessed fuel discharged after a typical LWR once-through fuel cycle. The decay heat to the repository is in proportion to the number of reprocessing steps, which varies inversely with the dpa limit. Clearly, a reduction in long-time decay heat to the repository of more than a factor of 10 could be accomplished by recycling the TRUs in LWR spent fuel in SABR. While the decay heat is inversely proportional to the dpa limit, Fig. 12 indicates that a substantial factor of 10 reduction is achievable with a radiation damage limit of 100 to 200 dpa, and it is not critical to increase the dpa limit further in order to make transmutation of TRUs realistic.

The initial calculations for fuel residence versus radiation damage were done assuming a fuel smear density of 100% and no rotation of fuel assemblies with shuffling (i.e., the same face of the assembly would be located inboard as the assembly was shuffled from the outermost to the innermost ring over the fuel cycle). The calcula-

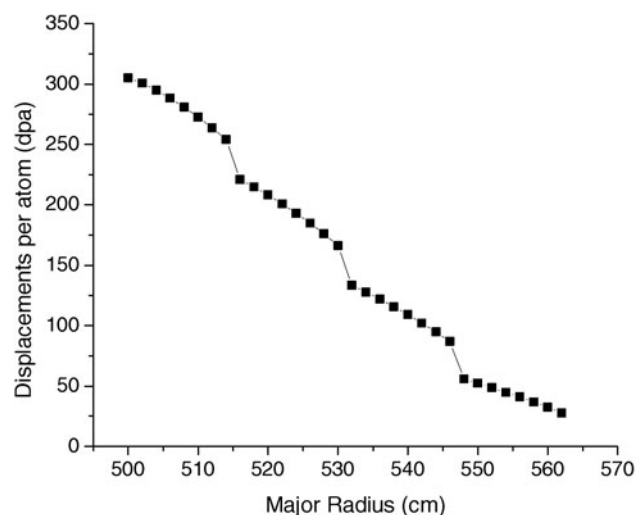


Fig. 11. Displacements per atom at end of the 300-dpa equilibrium fuel cycle.

tions on the reference 200-dpa cycle were repeated to investigate the effect of (a) utilizing a smear density of 95% to accommodate fuel swelling and expansion, and of (b) rotating the fuel assemblies by 180 deg each time they were shuffled. The results are summarized in Table V.

The effect of rotating the assemblies is minimal; the regional power peaking and the radiation damage are reduced by  $\sim 2\%$  and  $3\%$ , respectively, while the rest of the parameters remain the same.

The effect of changing the fuel smear density (a proxy for the total heavy metal mass) has a significant impact on the fuel cycle. The major effect of lowered heavy metal mass is a reduction in multiplication constant  $k$ , with a corresponding increase in the required fusion power  $P_{fus} = \text{const} (k/(1-k)) P_{fis}$ . The decrease in heavy metal mass also reduces the amount of waste to the repository and the amount of decay heat to the repository both by  $\sim 5\%$ .

#### IV.B. Minor Actinide Burner

The MA burner fuel cycle analysis emphasizes fissioning the MAs in spent fuel while setting aside the plutonium for other uses, as specified in the European studies of reactors to burn MAs (Ref. 7). The same 200-dpa, four-batch-with-rotated-assembly fuel cycle described in Sec. III was analyzed for both the MA-oxide and the MA-metallic fuel burner fuel cycles (see Table VI). The fuel cycles were evaluated based on the same criteria as used for the TRU burner fuel cycle.

The change in reactivity throughout the fuel cycle is greater in the oxide fuel because more plutonium is burned. This requires a greater change in fusion power from beginning of cycle (BOC) to EOC for the MA-oxide fuel. The fusion power required to maintain 3000-MW of

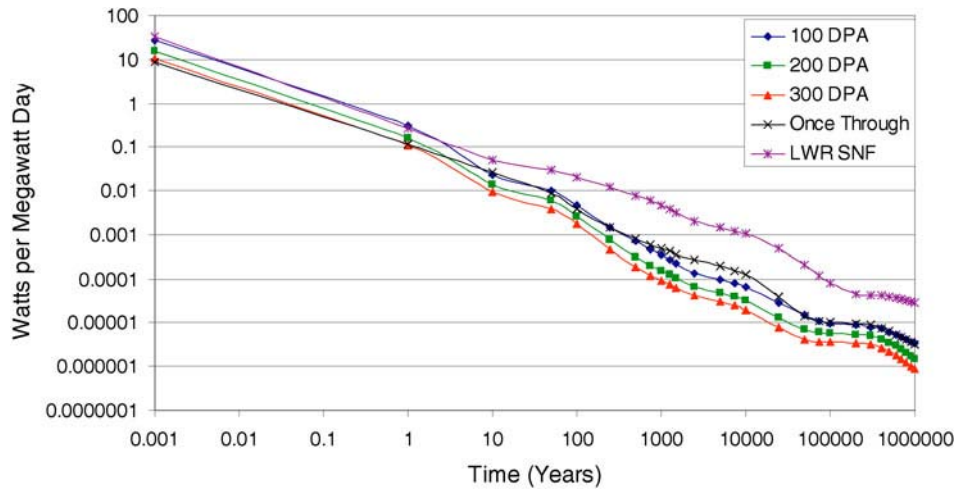


Fig. 12. Decay heat to the repository.

TABLE V  
Comparison of Rotated and Nonrotated 200-dpa Fuel Cycles with Metal Fuel

	200 dpa Rotated (95% Density <sup>a</sup> )	200 dpa Nonrotated (95% Density)	200 dpa Nonrotated (100% Density)
Fission power [MW(thermal)]	3000	3000	3000
BOL mass (kg HM)	30254	30254	31846
FIMA (%)	25.6	25.6	24.1
Region power peaking BOC/EOC	1.7/1.9	1.7/1.9	1.8/2.0
BOL $P_{fus}$ (MW)	172	172	73
BOC $P_{fus}$ (MW)	302	317	240
EOC $P_{fus}$ (MW)	401	429	370
BOL $K_{eff}$	0.945	0.945	0.972
BOC $K_{eff}$	0.878	0.863	0.894
EOC $K_{eff}$	0.831	0.817	0.868
Cycle reactivity change (pcm)	-6441	-6526	-3351
TRUs burned/yr (kg)	1027	1023	1064
Support ratio (100%)	4.1	4.1	4.2
Support ratio (75%)	3.1	3.1	3.2
Clad damage (dpa)	212	218	214

<sup>a</sup>The high values of the smear density are perhaps unrealistic, so the heavy metal mass is the relevant fuel parameter. The actual design (pin and assembly) sizes would be somewhat different than the fuel design given in this paper in lower-smear-density designs.

thermal power in the core varied from  $P_{fus} = 200$  to 500 MW in these fuel cycles, and the rate of MA fission (destruction) was 850 and 675 kg per effective full-power year for the metal form and the oxide form of the fast reactor fuel, respectively.

The TRU transmutation rate for the MA fuel is 1089 kg/yr for the metal fuel and 1122 kg/yr for the oxide fuel. The metal fuel burns more MAs than the oxide fuel; 78.3% of the TRUs burned in the metal

fuel are MAs compared to 58.9% of the TRUs burned in the oxide fuel. This is because the metal fuel is in a harder spectrum, making the fission cross section of the MAs more competitive with the fission cross section of the plutonium in the system. The normalized flux spectra for the oxide fuel and the metal fuel are shown in Fig. 13.

The neutron transport calculation treats the fusion neutrons as a volume source in the plasma region just

TABLE VI  
Minor Actinide Burner Fuel Cycle Comparisons

	Minor Actinide– Metal Fuel	Minor Actinide– Oxide Fuel
Fission power [MW(thermal)]	3 000	3 000
Four-batch residence time (yr)	7.67	7.67
BOL mass (kg HM)	49 985	47 359
BOC mass (kg HM)	48 468	45 658
EOC mass (kg HM)	46 441	43 542
Delta mass (kg)	2 027	2 110
Loading outer (kg)	13 040	12 345
Heavy metal out (kg)	11 013	10 234
FIMA (%)	15.5	17.1
Region power peaking BOC/EOC	1.5/1.6	1.3/1.5
BOL $P_{fus}$ (MW)	489	515
BOC $P_{fus}$ (MW)	190	195
EOC $P_{fus}$ (MW)	246	325
BOL $K_{eff}$	0.889	0.909
BOC $K_{eff}$	0.949	0.959
EOC $K_{eff}$	0.932	0.936
Cycle reactivity change (pcm)	−1 922	−2 552
TRUs burned/yr (kg)	1 089	1 122
Minor actinides burned/yr (kg)	853	674
Plutonium burned/yr (kg)	236	469
Uranium generated/yr (kg)	31	21
Ratio of decay heat to LWR SNF decay heat at 100 000 yr	0.10	0.10
Support ratio (100%)	34.1	27.0
Support ratio (75%)	25.6	20.2
Clad damage (dpa)	203	201

inboard of the annular subcritical multiplying fission core region, both surrounded by reflectors and shields. The fusion neutrons slow down, cause fissions and  $(n, 2n)$  reactions, which produce neutrons, which slow down and cause more fissions and  $(n, 2n)$  reactions, etc. The fusion source neutrons cause the spike in the group containing 14.1 MeV, which is more pronounced adjacent to the plasma source. The spectra shown in Fig. 13 are for a location in the middle of the first ring adjacent to the plasma source.

The spectral differences in the metallic and the oxide fuel cores are dictated by the competition of two effects—the fuel-to-coolant ratio and the amount of matrix material. The metallic fuel, with  $\sim 0.35$  cm<sup>2</sup> of coolant per pin, has a much larger fuel-to-coolant ratio than the oxide fuel, with  $\sim 0.69$  cm<sup>2</sup> of coolant per pin, which tends to make the spectrum harder in the metal fuel. On the other hand, the metal fuel has  $\sim 60\%$  matrix material, while the oxide fuel has  $\sim 45\%$  matrix material, which tends to make the oxide spectrum harder. The harder spectrum for the metal fuel is a result of the metal fuel design having a tighter lattice and less coolant per fuel pin than the oxide fuel design. The larger percentage of matrix mate-

rial in the metallic fuel than in the oxide fuel is more than compensated for by the smaller amount of coolant per pin for the oxide fuel design, resulting in a harder spectrum for the metallic fuel. Except immediately adjacent to the fusion neutron source, the neutron spectrum is more determined by the core composition than by the original energy of the neutron source (fission or fusion), so that the spectrum in SABR is very similar to what it would be in a critical IFR with the same core composition.

The LWR support ratio for the MA burner fuel cycle is defined as the ratio of MAs burned in SABR to the amount of MAs produced in a 1000-MW(electric) LWR, typically  $\sim 25$  kg of MAs/yr (Ref. 19). Note that this definition of support ratio for MA burning is different than the definition for TRU burning used previously. The LWR support ratios for the SABR metallic and European oxide fuels, assuming 75% availability, are 25.6 and 20.2, respectively, 1000-MW(electric) LWRs supported by a single SABR.

The decay heat to the repository in this system is very similar for both the oxide fuel and the metallic fuel; the overall burnups are 17.1% and 15.5%, respectively, reducing the need for repository capacity by 8.08 and 7.91 for

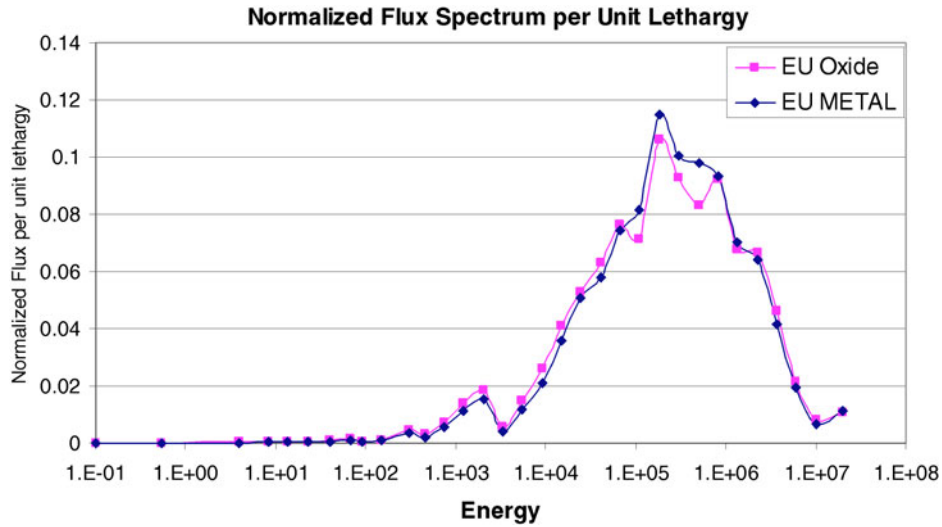


Fig. 13. Normalized flux spectra for MA-oxide and MA-metallic fuels.

the oxide system and the metallic system, respectively, not accounting for the plutonium that has been set aside for further use in mixed oxide or fast reactor systems. The decay heat to the repository in both of these cases is shown in Fig. 14, together with the heat that would be produced if the LWR spent fuel was just placed in the repository.

The rest of the evaluation criteria—power peaking, radiation damage, and overall TRU destruction rate for the metallic fuel and the oxide fuel in the MA burning cycle—were all very similar throughout the fuel cycle. This is a result of the fuels having similar BOL, BOC, and EOC reactivities and fusion powers. The oxide fuel performs better in terms of overall burnup, 17.1% to 15.5% for the oxide fuel and the metallic fuel, respectively.

The MA fuels have very similar fuel cycle performances in SABR. The biggest difference is in the ratio of

transmutation of MAs to the transmutation of plutonium. The choice of metallic- or oxide-fueled MA burners would be determined by this as well as by how each fuel performs in regard to safety in an accident scenario.

### V. SUMMARY AND CONCLUSIONS

We have investigated two types of fuel cycle for a SABR consisting of an annular, Na-cooled fast reactor surrounding a tokamak fusion neutron source. The first fuel cycle type is one in which all of the TRUs in LWR SNF are transmuted in a SABR, and the second fuel cycle type is one in which some of the plutonium in LWR spent fuel is set aside for future use and the remaining pluto-

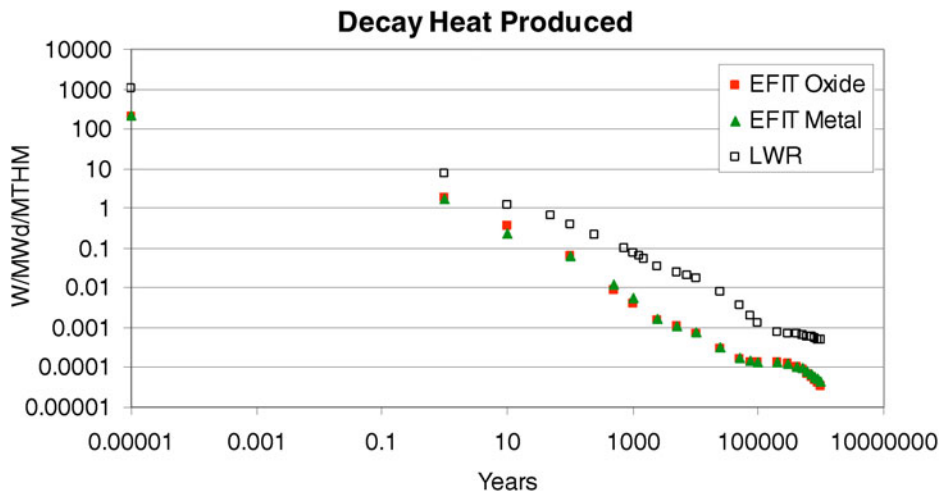


Fig. 14. Decay heat to the repository for MA burner oxide and metallic fuels.

niun plus the MAs are transmuted in a SABR. In both fuel cycle types, the fuel residence time between reprocessing steps was set by radiation damage limits (200 dpa reference value), and the separation of TRUs from fission products was assumed to be only 99% efficient. We found that, by repeated recycling of the TRU fuel discharged from SABR with a blend of fresh TRUs discharged from LWRs, the decay heat of the repository content could be reduced by a factor of  $\sim 10$  at 100 000 yr relative to the decay heat if the discharged fuel from LWRs was buried directly. Noting that decay heat load was the limiting design factor for Yucca Mountain capacity, this reduction in decay heat implies a corresponding reduction by a factor of 10 in HLWR capacity requirement. This result is based on the conservative assumption that the actinide-fission product separation efficiency is only 99%. We note that there are other measures (e.g., Sr and Cs management and cooling before storage) for reducing the required repository capacity, and they are not incompatible with the transmutation solution proposed in this paper.

A 3000-MW(thermal) SABR operating on such fuel cycles, with 75% availability, would be capable of burning all of the TRUs discharged annually from 3 LWRs of 1000 MW(electric), or burning all of the MAs and some of the plutonium discharged from 20 to 25 LWRs of 1000 MW(electric). Thus, one could envision a nuclear fleet with 75% of the energy produced by LWRs and 25% of the energy produced by SABRs that burned all of the TRUs discharged from the LWRs. Alternatively, one could envision a nuclear fleet with 95% of the energy produced by LWRs and 5% produced by SABRs that burned the MAs (primarily) and some of the plutonium discharged from LWRs, while plutonium was accumulated to start up fast reactors.

## REFERENCES

1. "Waste Management Background," Office of Civilian Radioactive Waste Management: <http://www.ocrwm.gov> (current as of July 9, 2012).
2. "Expected New Reactor Applications," Nuclear Regulatory Commission: <http://www.nrc.gov/reactors/new-reactors/new-licensing-files/expected-new-rx-applications.pdf> (current as of July 9, 2012).
3. *Proc. Int. Information Exchange Mtg. Actinide and Fission Product Partitioning and Transmutation*, mtgs. 1 through 10, Organisation for Economic Co-operation and Development, Nuclear Energy Agency (1990–2008).
4. E. A. HOFFMAN and W. M. STACEY, "Comparative Fuel Cycle Analysis of Critical and Subcritical Fast Reactor Transmutation Systems," *Nucl. Technol.*, **144**, 83 (2003).
5. C. M. SOMMER, W. M. STACEY, and B. PETROVIC, "Fuel Cycle Analysis of the SABR Subcritical Transmutation Reactor Concept," *Nucl. Technol.*, **172**, 48 (2010).
6. W. M. STACEY et al., "SABR Fusion-Fission Hybrid Fast Burner Reactor Based on ITER," presented at 11th Information Exchange Mtg. Actinide and Fission Product Partitioning and Transmutation, San Francisco, California, November 1–4, 2010, Nuclear Energy Agency.
7. V. ROMANELLO et al., "Advanced Fuel Cycle Scenario Study in the European Context by Using the SABR Hybrid Fusion-Fission System," presented at 11th Information Exchange Mtg. Actinide and Fission Product Partitioning and Transmutation, San Francisco, California, November 1–4, 2010, Nuclear Energy Agency.
8. C. ARTIOLI et al., "Minor Actinide Transmutation in ADS: The EFIT Core Design," presented at Int. Conf. Physics of Reactors, Interlaken, Switzerland, September 14–19, 2008.
9. W. M. STACEY et al., "A TRU-Zr Metal-Fuel, Sodium-Cooled Fast Subcritical Advanced Burner Reactor," *Nucl. Technol.*, **162**, 53 (2008).
10. N. HOLTkamp, "The Status of the ITER Design," *Fusion Eng. Des.*, **84**, 98 (2009).
11. C. E. TILL, Y. I. CHANG, and W. H. HANNUM, "The Integral Fast Reactor—An Overview," *Prog. Nucl. Energy*, **31**, 1 (1997).
12. S. HAYES and M. MEYER, Argonne National Laboratory, Personal Communication (2007).
13. J.-P. FLOYD et al., "Tokamak Fusion Neutron Source for a Fast Transmutation Reactor," *Fusion Sci. Technol.*, **52**, 727 (2007).
14. G. RIMPAULT et al., "The ERANOS Code and Data System for Fast Reactor Neutronic Analyses," Proc. Int. Conf. New Frontiers of Nuclear Technology: Reactor Physics, Safety and High-Performance Computing (PHYSOR 2002), Seoul, South Korea, October 7–10, 2002, American Nuclear Society (2002).
15. C. GHO and G. PALMIOTTI, "BISTRO: Bidimensionnel sn transport optimize, un programme bidimensionnel de transport sn aux differences finies note nl definition des algorithmes pour la geometrie x-y," technical report.
16. J. Y. DORIATH et al., "Eranos Manuel Des Methodes—Les Calculs D'Evolution," CEA.
17. A. BOPP, Georgia Institute of Technology, Personal Communication (2011).
18. "SCALE: A Modular Code System for Performing Standardized Computer Analyses for Licensing Evaluation," ORNL/TM-2005/39, Version 5.1, Oak Ridge National Laboratory.
19. F. GOLDNER and R. VERSLUIS, "Transmutation Capabilities of GEN-IV Reactors," September 2006; [http://www.nea.fr/html/pt/iempt9/Nimes\\_Presentations/GOLDNER4.pdf](http://www.nea.fr/html/pt/iempt9/Nimes_Presentations/GOLDNER4.pdf) (current as of July 9, 2012).